Automated Microchannel Alignment Using Innate Opto-Signature for Microchip Electrophoresis

Journal:	*Lab on a Chip*
Manuscript ID	LC-ART-07-2019-000716.R1
Article Type:	Paper
Date Submitted by the Author:	29-Aug-2019
Complete List of Authors:	Scott, Anchi; University of Virginia, Department of Chemistry Mills, Daniel; TeGrex Technologies Birch, Christopher; University of Virginia, Department of Chemistry Panesar, Satvinder; TeGrex Technologies Li, Jingyi; University of Virginia, Nelson, Daniel; University of Virginia Startseva, Margarita; TeGrex Technologies Khim, Albert; TeGrex Technologies Root, Brian; University of Virginia, Applied Research Institute Landers, James; University of Virginia, Department of Chemistry

SCHOLARONE™
Manuscripts

ARTICLE

Automated Microchannel Alignment Using Innate Opto-Signature for Microchip Electrophoresis

Anchi Scott,[a] Daniel Mills,[b] Christopher Birch,[a] Satvinder Panesar,[b] Jingyi Li,[a] Daniel Nelson,[a] Margarita Starteva,[b] Albert Khim,[b] Brian Root,[c] and James P. Landers [a,d,e]

In laser-induced fluorescence (LIF) detection, optimal alignment is essential in maximizing the fluorescent signal and, hence, detection sensitivity. Micro-total analysis systems (μTAS) involving microchip electrophoresis (ME) are challenged with alignment of the optics to the separation channel each run due to the single-use nature. Furthermore, μTAS devices that are designed to operate autonomously and by non-experts face additional challenges in performing alignment with micrometer resolution without human intervention. As part of the development of a total DNA anlysis system, we set out to develop an automated alignment (AA) method to locate a 50-by-50 μm separation channel on a freely rotating microfluidic device in the absence of a fluorescent dye, accomplished without additional hardware. We detail the innate fluorescent signature attainable from laser excitation and the optimization of the algorithm to achieve AA at 92% success rate from 26 microchips. This AA method was a key element in realizing complete automation of the DNA analysis process in order to advance our instrument to a technolgoy readiness level of 7. This is the first description of an AA method for ME (and centrifugal ME) with the purpose of providing transparent technical details to bridge the gap from 'fully integrated' to 'fully automated' instruments for point-of-detection, sample in-answer-out use cases. Written in the context of a forensic application, the AA method is adaptable for a wide range of bioanalytical applications invovling LIF detection.

Introduction

Automation is a key qualification towards intervention-free operation of lab-on-chip (LOC) devices or a micro-total analysis systems (μTAS). On the scale of Technology Readiness Level (TRL) (a term developed at NASA to assess the maturity of a technology), automation may be the developmental goal and defining feature that transcends a technology from the early proof-of-concept (TRL3) phase to the mature prototype (TRL7) phase equipped to handle its intended operating environment. For example, a challenge with robotic analytical devices for *in situ* planetary exploration[1] (assuming the instrument survives spaceflight and unpredictable extra-terrestrial environments), complete autonomous operation is required to analyze organic molecules using capillary electrophoresis by laser-induced fluorescence (LIF). This is further complicated by the requirement of a sample acquisition step that is generally considered an inevitable manual step in forensic and clinical microfluidic applications. Consequently, fully automated spaceflight devices generally reside at TRL3 and TRL4 as reviewed by Willis et al[1].

Arguably the best terrestrial example for automation is the analysis of DNA evidence to generate a DNA profile (civil and military). 'DNA typing' by short random repeats (STRs) is a gold standard process in human identification since around 1993[2], whereby DNA evidence undergoes DNA extraction, amplification, separation and LIF detection to generate a DNA profile up-loadable to a national database. Modern DNA typing chemistries can consistently amplify as little as 0.25 ng DNA (~40 diploid cells)[3], allowing the detection of low copy number samples often present in forensic applications. Although powerful and reliable, the labor-intensive process requires highly skilled personnel and multiple specialized equipment conducted under a controlled operating environment. In addition, the ever-increasing DNA evidence submitted created a high demand for rapid and full automation of DNA typing in the early 2010s[4]. Such a device/instrument, termed 'Rapid DNA', would be portable, operable by a non-expert user in an environment other than a forensic laboratory, and perform DNA typing without human intervention in under 2 hours[4].

One can start to appreciate the complexity of Rapid DNA by examining the separation and detection sub-processes alone. To confer high discriminatory power in DNA typing to identify or exclude subjects of interest, up to 24 markers are amplified in a single PCR reaction, which are labeled with one of five different fluorescent probes to utilize the region of best separation resolution (1 base). Traditionally, following PCR, fluorescently-labelled DNA fragments are electrophoretically separated in a glass capillary with single base resolution and the multi-colored fluorophores detected with high sensitivity. Applied Biosystems 310 (*ABI 310*) is an early exemplary

a. Department of Chemistry, University of Virginia, Charlottesville, VA 22904, USA. Email: landers@virginia.edu
b. TeGrex Technologies, Charlottesville, VA 22903, USA.
c. Applied Research Institute, University of Virginia, Charlottesville, VA 22904, USA.
d. Department of Mechanical and Aerospace Engineering, University of Virginia, Charlottesville, VA 22904, USA.
e. Department of Pathology, University of Virginia, Charlottesville, VA 22904, USA.

instrument which can automatically process up to 96 samples by injecting one sample at a time through the single capillary setup (at 45 min per sample). *ABI 3130 xl* is a newer model which increases the throughput by incorporating a 16-capillary array. The former instrument requires a capillary change by the user after 100 runs, whereas the latter requires a technician to perform the array change after 1000 runs. In addition, whenever a new capillary array is installed or the instrument is moved, a laser alignment and spectral calibration are performed by the technician to ensure optimal detection efficiency. Considering the learning curve required to master capillary change and optical alignment, and the said portability of Rapid DNA, the maintenance component associated with CE-based separation and detection is not construed as automation-friendly.

Microchip electrophoresis (ME), on the other hand, is particularly suited for microfluidic, single-use, sample in-answer out scenarios. Agilent's Bioanalyzer is perhaps the most well-known commercialized ME device (TRL 9), where a glass separation domain (the 'capillary') is interfaced with a 12-sample plastic casing to perform nucleic acid or protein fragment analysis. Facing the challenge of the disposable nature of the microchip requiring optical alignment each run, the chip is spring-loaded onto the platform, followed by auto-alignment and auto-focusing using stepper motors to achieve optimal fluorescence detection (based on limited literature description[5]). One commercialized Rapid DNA instrument, *ANDE* (formerly *DNAScan*), is described to have a lane-finding algorithm to automatically find the ME channel each run[6]. Another common approach for optical alignment involves filling the separation channel with a fluorescent dye, then scanning laterally (across the channel) and vertically (focusing plane) to find the maximal fluorescence signal. This was the strategy described in a TRL7 Rapid DNA instrument described by Le Roux et al[7], where a high wavelength dye (outside the spectra of the PCR fluorophores) was incorporated in the electrophoresis buffer and, by finding the maximum dye signal through y- and z-axis rastering, optimal channel alignment was identified. Other attempts at evaluating the literature on ME channel alignment found scant reports of an alternative approach. For example, Hopwood described a forensic DNA analysis system where "*alignment and focusing of the chip and detection system was achieved by a push-button activated servo motor and a micrometer screw respectively, on a 3 mm translation stage*"[8]. Other reports in the public domain included a method that used Raman scatter signals[9], and another that aligned the channel based on the capillary wall scatter pattern[10]. The necessity for automated alignment is obviously profound but the technical details needed for execution safe-guarded. In addition, the limited literature in the public domain remains largely enigmatic in terms of effectiveness and usefulness in praxis.

Herein, we dedicate a detailed report on an automated method for the accurate and precise alignment of optics to a 50 x 50 µm ME channel on a centrifugal platform. The automated alignment (AA) method is part of the development of a Rapid DNA instrument, named *faSTR*, which coordinates DNA extraction, STR amplification, electrophoretic separation and LIF detection from a buccal sample to generate a DNA profile in under an hour (manuscript in prep[11]). Centrifugal microfluidic affords drastic volumetric and weight reductions (and thus better portability) by eliminating pumps and tubings. However, the freely rotating microchip adds a layer of complexity and challenge associated with ME (no fixed clamp position) in addition to the compulsory optics alignment imposed on single-use, point-of-detection use cases. Nevertheless, we report an AA method that does not require the presence of a fluorescent dye in the separation sieving matrix, but instead relies on the innate optical signatures, hence 'opto-signature', emitted from the channel features during excitation. Therefore, no additional hardware is required other than the optical system already employed for LIF detection. We shed insight into a novel strategy and the associated method optimization processes for AA. We characterized the effect of slight mis-alignment on signal intensities, and report the reproducibility, limitations and success rate of the method. Although developed in the context of forensic DNA analysis, the method can be viewed as a 'plug-and-play' strategy for any analytical application requiring LIF and, hence, potentially enabling anyone looking to achieve total automation.

Experimental

Microchip fabrication

The centrifugal microchip for performing integrated DNA liberation, amplification, separation, and detection was fabricated using the general Print-Cut-Laminate (PCL) method described by Thompson et al[12]. Fabrication and assembly of the separation domain specifically was described previously[13, 14]. Briefly, the microchip was assembled from multilayers of mixed substrates, each layer was laser ablated to convey microfluidic architecture before bonding via heat sensitive adhesive. The separation domain contained an injection molded layer to which electrophoretic separation of DNA fragments occurred was bonded to the microchip via pressure sensitive adhesive. The microchip measured 66 mm in diameter, 0.55-6.95 mm in height depending on the domain features, and weighted 36.6 g with all reagents on board inside a light- and humidity-protective packaging.

Instrumentation

The fully automated and fully integrated µTAS or Rapid DNA instrument, named *faSTR*, consists of all hardware, control software, and user interface in the form of a touchscreen to operate DNA analysis. Once sample (buccal swab) is sealed into the chip, the chip is clipped onto the chip mount just as a music CD, and all subsequent operations are carried out in a fully automated fashion, in an enclosed aluminum shell to provide a light-tight environment for laser-induced fluorescence (LIF) detection. Instrumentation details are described elsewhere (manuscript in prep[11]). Subsystems pertinent to this report include: (1) a brushed DC spin motor to conduct centrifugally-

driven microfluidic control, (2) a photo-interrupter to locate rotational positions on chip, (3) a 638 nm laser to actuate normally closed valves, (4) a geared, brushed DC clamping motor to which the microchip will be engaged by the gold spring-loaded pogo pins for electrophoretic separations, (5) a custom high voltage power supply to step 12V to 2kV using DC-DC regulators, and finally (6) the optics subsystem. The excitation source is a laser diode at 488 nm (60 mW), delivered orthogonally to the plane of the detection window affixed on an X-Z motorized linear translation stage with fine adjustment of 5 μm (where 1 μm = 7 encoder counts) (**Figure 1A**). Fluorescence emission is then filtered through a series of mirrors and filters and collected by a Hamamatsu 4 channel linear multi-anode PMTs (photomultiplier tubes). The fluorescence probes used in this study were FAM (518 nm), JOE (548 nm), F3TMR (578 nm), and WEN (671 nm). Individual voltage signals were then passed through an 8-pole Butterworth low pass filter to eliminate spurious high frequency noise, amplified, and digitized using the microcontroller's on-board peripheral analog-to-digital converter. Digital signals are logged and displayed to the touchscreen in real time. The automated channel alignment, high voltage control, and data collection processes are coordinated by commands issued from a PC-based graphic user interface (GUI) to an ARM microcontroller and custom printed circuit board located inside the syste. This allows the user to create custom series of instructions using a generalized scripting command set. The GUI was developed in Visual Basic and embedded software was written in C.

Optimization of alignment strategy and algorithm

The basic strategy for automated alignment (AA) involves four steps: (1) conduct 50 scans by moving the X-Z motor at an increment of 25 μm in Z height (total coverage 1.25 mm) starting from the upper most focal point, each scan encompasses 1 mm in the X direction (**Figure 1D**); (2) find the optimal Z height by determining the inflection point from the processed signal (**Figure 2B**) and apply an offset; (3) find the optimal X location by identifying the scan of interest (SOI), to which the absolute minimum and a local maximum are recognized by the algorithm (**Figure 2D**); and (4) an offset is applied to the X location before moving the optics to optimal Z and X location. The time to complete AA was under 4 min, which was primarily the time required for the motor to conduct the scans, steps 2-4 were executed within seconds.

The first essential parameter to optimize AA was the PMT gain to which the color channel that alignment signals are collected from. In this case, the red channel (F3TMR) was selected for its wide dynamic range and low noise. Equally important, is the optimization of scan starting positions and the total distance scanned for both directions to ensure coverage of the height and width of the 50 x 50 μm channel. All parameters were determined empirically from thirty-eight microchips over four weeks with minor modifications to fine-tune the final algorithm.

Alignment output data from each AA was generated upon completion, which contains the raw signal for 50 scans at each Z height across the X direction (in encoder count). The output also contains the processed signal which is the averaged signal per Z scan (filtered for outliers), to allow the analysis of Z location accuracy by graphing the processed signal versus the scan number (as seen in **Figure 2B**). The scan number associated with the inflection point is where the final Z and X scans are determined from. Pertinent parameters to analyze X location accuracy include those searched by the algorithm, i.e., absolute minimum, local maximum, and final X location in encoder count. Graphing and logging of these parameters help record and troubleshoot AA throughout the optimization and the final analysis for the integrated runs.

Microchip electrophoresis

Microchip electrophoresis (ME) of PCR product is performed either as part of an integrated run (DNA extraction, amplification, separation and LIF detection) or as a stand-alone assay on the *faSTR* system. The 10-plex PCR markers target the short tandem repeat regions in human Amelogenin, D3S1358, D21S11, D7S820, D16S539, D18S51, D2S441, D12S391, D13S317, and TPOX. These are selected from the core set of markers demanded by the FBI for submitting DNA profiles to national or international databases for human identification.[15] Chromosomal location and primer sequences are detailed by National Institute of Standards and Technology.[16]
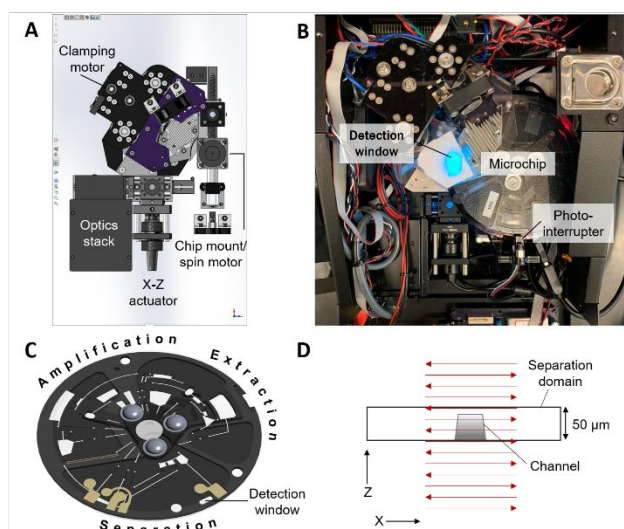
Figure 1 - Automatic alignment hardware and strategy. (A) Top view schematic of the of optics hardware to perform alignment and microchip separation. (B) Top view of the system without the front panel to show the microchip engaged by the clamping motor, and the excitation source through the detection window. (C) Schematic of the integrated microchip with three assay domains. The detection window, measures 3 x 8 mm at its widest points, is labelled. (D) Side view of the scanned region in the X and Z spatial directions relative to the separation channel.
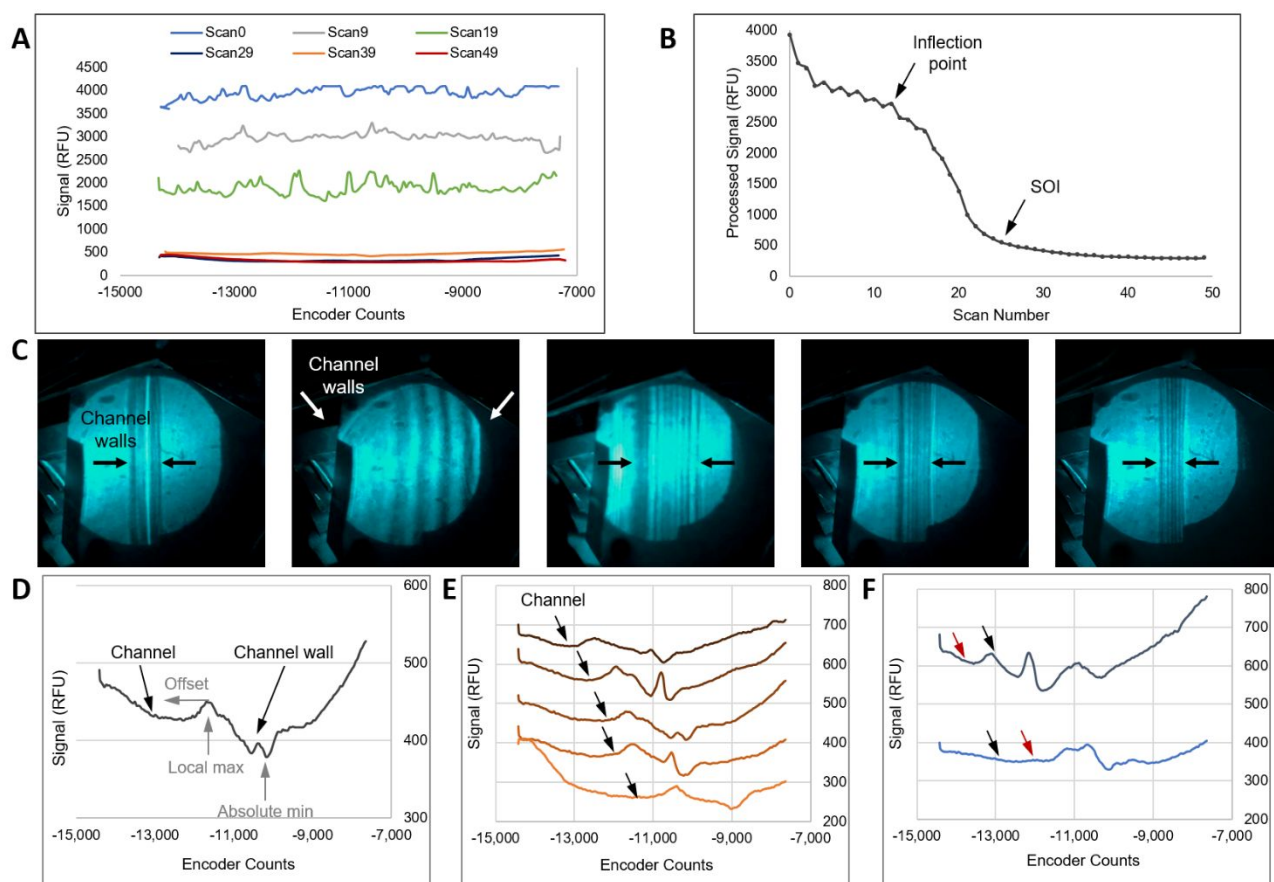
Figure 2 – Raw or processed signals for locating the optimal Z and X positions. **(A)** Raw signals from Z scans at 5 different Z heights. **(B)** Processed signal from 50 Z scans producing a characteristic sigmoidal-like curve. **(C)** Top view of the separation channel at scan numbers 0, 9, 19, 29, and 39 (left to right) as shown in **(A)**. **(D)** A representative raw signal in the SOI for finding the channel in the X direction. The signature traits recognized by the algorithm are labelled in grey. **(E)** Five traces in the SOI that enabled the accurate location of the separation channel in the X direction (black arrows). **(F)** Two traces that resulted in alignment failures in the X direction, where black arrows indicate the ideal location and the red arrows indicate the found location.

During an integrated run, a novel hydrophobically-modified polyacrylamide polymer[7] was loaded interspersed throughout prior assays via centrifugal force. To perform ME alone, polymer loading is achieved by applying 3,000 RPM for 10 min,
5 followed by the actuation of two laser valves to establish electrical connectivity between the via and the sample waste (SW) and buffer (B) electrodes. A third laser valve is actuated to allow the sample (containing pre-mixed PCR product and ILS heated at 95°C for 3 min and snap cooled on ice for 3 min) to
10 be connected with the sample (S) electrode. Once fluidic movement is complete, the microchip is located rotationally via the photo-interrupter, and clamped by the clamping motor to establish contact between the gold pogo pins with the electrode pads on the microchip. Electrophoretic injection is
15 performed at 500V (700 V/cm) for 60 sec from S to SW electrodes, and separation at 1500V from B to BW with a pullback voltage applied at 200V at S and SW for 450 sec (250 V/cm). During an integrated run, injection is performed instead at 600V (850V) for 30 sec from S to SW electrodes, followed by
20 gating the sample plug at 1500V for 2 sec from S to BW (buffer waste), before separation conditions are applied as described. The effective length of separation (cross T to detector) is 6 cm. The operational steps involved in an integrated run compared to a stand-alone ME run are summarized in the supplementary
25 information.

Data analysis

At the completion of ME, integrated data analysis is performed on the µTAS through a data analysis pipeline, which
30 involves trimming of primer peaks, baseline subtraction, pullup correction, and amplifying the signal 10x using a digital filter. Smoothing was also done using a Fast Fourier Transform and an Inverse Fast Fourier Transform. The processed data is then re-formatted and saved as a ".txt" for compatibility with
35 Microsoft Excel, as well as a ".fsa" file for forensic analysis in GeneMarker.

Processed data from each ME run is analyzed in GeneMarker for fragment sizing and allele calling prior to outputting the peak height as a ".txt" file. The peak height is
40 either averaged for a heterozygous marker or halved for a homozygous marker. The processed peak height for a given marker is averaged across the replicated ME runs and shown in **Figure 3B**, and further averaged for a given color across the replicated ME runs and shown in **Figure 3C**. Standard deviation
45 of the replicates are shown as error bars in **Figure 3**. The noise of the red channel was calculated by the standard deviation of 50 datapoints flanking the ILS fragments at 140, 200, and 300

bases under each alignment scenario. Consequently, the signal-to-noise ratio (SNR) is calculated by the proportion of the peak height of the perspective ILS fragment over associated noise. An analytical threshold was determined to be 134 RFU, as
5 calculated from 10x the highest noise.

Results and Discussion

Instrument hardware and alignment strategy

Automatic alignment (AA) is conducted with hardware already built-in for LIF detection, which are comprised of: (1) a
10 488 nm laser diode at 60 mW, (2) an X-Z actuator to permit movement with 5 μm increments, (3) an optics stack with mirrors and filters for collecting the desired wavelengths of four fluorophores, and (4) photomultiplier tubes (PMTs) for signal detection. Other hardware that are associated with AA
15 are shown in **Figure 1A&B**, which include the chip mount/spin motor coupled with a photo-interrupter to locate the rotational position (Y) of the detection window, followed by the engagement of the pogo pins to the electrode pads on the microchip via the clamping motor.
20 Although spatial alignment is required in all X, Y, and Z directions, the Y directional alignment was already achieved through the photo-interrupter by finding the detection window, which exposes the curved separation channel. Locating the X and Z positions were done through a series of
25 lateral scans (X axis) at different Z heights, shown in **Figure 1D**. The coverage for X and Z is 1 and 1.25 mm in total, respectively, to ascertain the separation channel is within the search. The resulting fluorescence signal from the scans, or simply 'signal' in later text, is acquired the same way as LIF detection of the
30 four fluorophores, and therefore is displayed as relative fluorescence unit (RFU).

Locating the optimal Z & X

Figure 2A shows the signal intensity (RFU) at each position
35 in the 'Z' direction (Z = height) during translation through the 'X' direction (across the width of the channel; motor encoder count). The raw signal across the X direction (6 scans shown in **Figure 2A**) was processed by averaging to yield a data point for a given Z height. The resultant, processed signal (**Figure 2B**) is
40 inversely proportional to the distance between the optics and the separation channel. As the laser spot comes into focus with the channel substrate (separation domain), the signal intensity is most responsive to the changing distance between the optics and the substrate, forming the sigmoidal portion of the Z scan.
45 From this processed signal shown in **Figure 2B**, the optimal Z height was empirically determined at 5 Z steps above the inflection point. When the optics are out of focus of the material, the signal intensity is relatively unchanged, which is explained by the plateau on either side of the sigmoid. Through
50 the detection window (without the aluminum cover of the system), the fields of view in **Figure 2C** correspond to the approximate Z heights at Scan 0 to 39 in **Figure 2A** (taken with X position aligned). An optimal Z alignment typically results with the channel walls outside the field of view (white arrows),

55 whereas suboptimal Z alignments can be seen with separation channel walls in view (black arrows).

The scan of interest (SOI) for finding the optimal X is located 13-14 Z steps below the inflection point (**Figure 2B**). As depicted in **Figure 2D**, the raw signal of the SOI is analyzed by
60 the algorithm to sequentially locate the 'absolute minimum', 'local max', and an 'offset encoder' value in order to find the center of the channel. These minor 'interference' signals, presumably from the distinct separation channel walls, form a reproducible pattern regardless of the injection molding batch
65 of the separation domain and type/batch of separation sieving matrix used. Although reproducible, **Figure 2E** highlights five examples of successful AA with highly variable 'absolute minimum' values (encoder position) and, subsequently, varied final X positions (black arrows). This suggests that the
70 methodology and the algorithm are tolerant to minute chip-to-chip variations (on the order of 100-200 μm), likely due to slippage in multilayer assembly during chip fabrication. In cases where an atypical raw signal is obtained from the SOI, the algorithm failed to identify the correct X position. The top trace
75 in **Figure 2F** mis-identified the absolute minimum, therefore defining a grossly incorrect X position that was to the left of the separation channel by ~980 encoder counts (~140 μm) (incorrect position, red arrow; correct position, black arrow). The bottom trace shows a similar problem where the local
80 maximum was mis-identified, this time resulting in an X position to the right of the separation channel by ~140 μm. From observation, imperfections such as bubbles trapped during injection molding, dust or fingerprints on the separation domain present in the scanning region can cause failures by
85 interfering with the channel signatures. Thus, standard operating procedure was to clean the detection window with ethanol and a dust-free wipe, followed by drying with compressed air prior to AA (or prior to an integrated run involving DNA extraction, amplification, separation and LIF
90 detection). A detection window in pristine conditions is often a requirement for LIF applications. Additional caution such as handling of the device with gloves and avoid touching the detection window, or a protective tape to seal the window until analysis is initiated can both be implemented in future designs.
95

Effect of mis-alignment on signal intensity

To establish a metric for determining when AA was successful, the effect of mis-alignment in the Z, X, or both Z and X directions on the intensity of the fluorescent signals was
100 systematically studied. A standard ME protocol described in the *Experimental* section was employed to ensure ME was reproducible (same PCR product, same volume etc.). Briefly, following polymer loading by centrifugal force, the microchip is aligned manually (or mis-aligned purposefully), before a
105 sample containing pre-amplified 10-plex PCR products (10 PCR markers) mixed with an internal lane standard (ILS) were injected and separated. The signal intensities collected from 4 fluorophores were analyzed and compared between four commonly-observed alignment scenarios. **Figure 3A** depicts
110 the alignment positions using schematic drawings from the
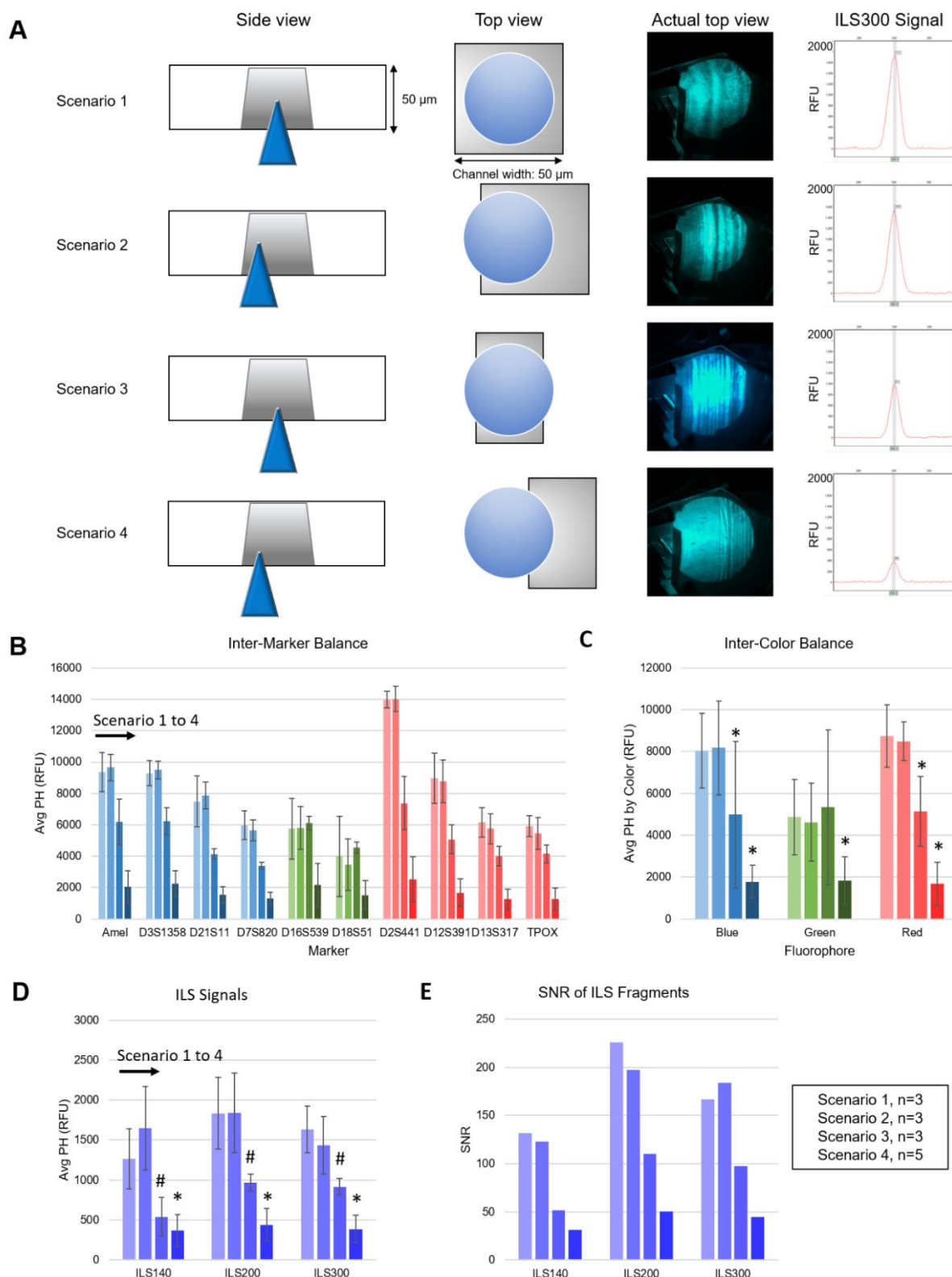
Figure 3 - Effect of mis-alignment on signal intensities. **(A)** Left to right, schematic of side and top view of the alignment positions in four common scenarios, actual top view of the separation channel through the detection window, and an example cropped electropherogram showing the peak height of ILS300. **(B)** Averaged peak height (PH) per locus obtained under 4 scenarios. **(C)** Averaged PH per color. **(D)** Averaged PH for three ILS fragments. **(E)** Signal to noise ratio (S/N) of ILS fragments. Error bars showing STDEV from 3 runs for Scenarios 1-3, and 5 runs for Scenario 4. Statistical analysis performed by Student t-test, where "**#**" denotes $p < 0.05$ and "*****" denotes $p < 0.01$.

side and top views (first and second columns, respectively),

followed by the actual top view through the detection window (third column), and an example peak height of the ILS fragment

at 300 bases (fourth column). Scenario 1 depicts an ideal alignment where the focal point is centered in the separation channel in both Z and X directions. Scenario 2 depicts an ideal Z position but 40% mis-alignment in the X direction, resulting
5 in a significant portion of the channel wall in the field of view. Scenario 3 depicts an ideal X position but 40% mis-alignment in the Z direction, which also resulted the channel walls dominating in the field of view. Scenario 4 depicts a mis-alignment in both the Z and X directions, resulting in a
10 significant loss in the area of separation channel in view.

Fluorescent signals detected at each PCR marker as a result of the alignment positions are shown as averaged peak heights from 3-5 runs (as specified in **Figure 3B**). The columns are color-coded based on the fluorophore 'color' and shown as
15 comparison from scenario 1 to 4 (left to right). The averaged peak height of the same fluorophore was further averaged and shown in **Figure 3C**. It is evident that signal intensities collected from Scenario 1 and 2 are comparable in all colors, suggesting that a mis-alignment by ~20 μm in the X direction led to
20 negligible loss in signal. However, Scenario 3 showed a statistically significant ($p < 0.01$, denoted as "*" on figure) loss in the blue and red signals by 38% and 41%, respectively. Mis-alignment in both Z and X directions as in Scenario 4 showed a signal loss of 77% in blue, 62% in green, and 81% in red.

25 In a similar fashion, three fragment sizes of ILS were chosen for peak height comparison under four alignment scenarios (same ME runs as **Figure 3B & C**). Averaged peak heights from multiple runs for ILS at 140, 200, and 300 bases are shown in **Figure 3D**. ILS140 was selected over ILS100 due to the varied
30 peak width at ILS100 that can sometimes occur, leading to a seemingly lower peak height (peak area would be a more suitable measurement in this case, but ILS140 was chosen for unit consistency). There was no statistical difference in signal intensities between Scenario 1 and 2 in all the ILS fragments,
35 consistent the results from other colors. In Scenario 3, however, there is a 44-57% decrease in signal compared to Scenario 1 ($p < 0.05$, denoted as "#"); or 70-76% decrease in Scenario 4 compared to Scenario 1 ($p < 0.01$, denoted as "*"). The signal loss in Scenario 3 and 4 corresponded to a drastic
40 decrease in signal-to-noise ratio (SNR), shown in **Figure 3E**, indicating a decrease in detection sensitivity as the alignment deviates greater from the center of the separation channel. The SNR for ILS fragments in this alignment study measured at least 30 even for Scenario 4, which is well above the SNR of 3 for
45 limit of detection (LOD) or SNR of 10 for limit of quantitation (LOQ).

The major finding from this study is that detection sensitivity is very tolerant of a mis-alignment in the X direction (Scenario 2), but substantially less so in the Z direction
50 (Scenario 3). The most significant signal loss occurred in Scenario 4, suffering a 62-81% decrease depending on the fluorophore. Interestingly, the study by Le Roux et al., found the maximum deviation tolerable in the Y and Z direction was 10 and 38 μm, respectively[7], whereas this study found it less
55 tolerable towards a deviation in the Z direction. During DNA profiling, the PCR peak heights generated from the unknown donor will inevitably vary based on DNA concentrations and

minor volume fluctuations from integrated microfluidic maneuvers, therefore the success metric for alignment can
60 only be determined based on the completeness and peak height of ILS fragments. In other words, the detection of ILS fragments up to 300 bases, and an analytical threshold of 134 RFU (as calculated from 10x the highest noise obtained from ILS channel in this study) must be met to be deemed successful.

65 **Reproducibility**

To understand the success rate of the AA strategy, 30 fully integrated DNA analysis runs were carried out on the *faSTR* system. However, 4 runs were eliminated due to poor separation conditions (e.g., bubble formation in the separation
70 channels), resulting in poor ILS signal to no fault of alignment). DNA lysis and amplification proceeded as normal, a brief pause was introduced to the run sequence post-AA, prior to ME, to visually assess and record the alignment position (no manual intervention). Nine runs were perfectly aligned (Scenario 1),
75 giving rise to strong fluorescent signals and ILS SNR well above 10. Fifteen runs were found to be mis-aligned in the X direction (Scenario 2), although all were deemed successful with the exception of one run. In that run, the raw X signal is shown in **Figure 2F** (top), and the resulting ILS signals are shown in **Figure**
80 **5A**. Despite achieving ideal Z coverage, i.e., scanning range, for all 26 runs (seen by the narrow range of inflection points, and thus optimal Z position in **Figure 4A)**, only two runs were found to be mis-aligned in the Z direction, and happened to also mis-align in the X direction (Scenario 4). One of these was within
85 the success metric while the other run was not. The proportion of Scenario 1 through 4 is plotted in **Figure 4B**, where the largest incidence of mis-alignment was Scenario 2 at 58%, but among which, only 1 run failed to meet metric. This is consistent with the data from the previous study (**Figure 3**),
90 where high tolerance for mis-alignment in the X direction was observed. There was no incidence of Scenario 3 in this dataset, though 8% of the runs were Scenario 4, which contained the
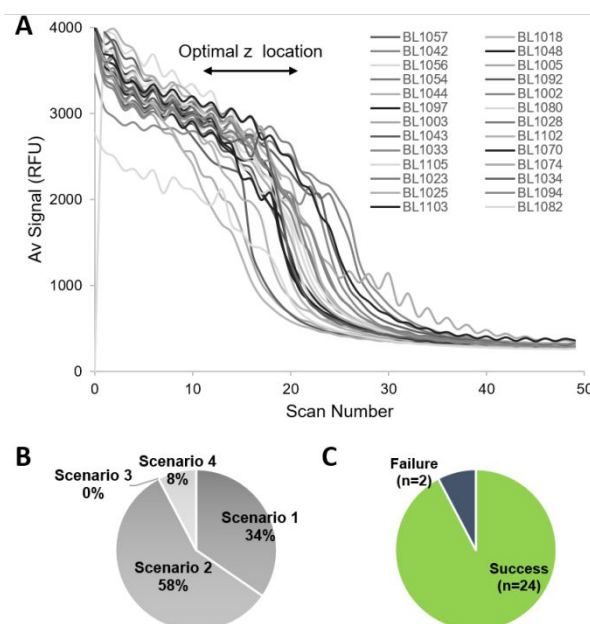
Figure 4 - Reproducibility and success rate of AA. (A) Scan Z coverage reproducibility from 26 fully integrated DNA analysis runs. (B) The proportion of each AA scenario. (C) Success rate of AA as determined by the ILS signal.

Please do not adjust margins
Lab on a Chip
Page 8 of 11

second failed run in this study. It is thought that the mis-alignment in the Z direction for this failed run was greater than the controlled study in **Figure 3**, resulting in less channel area under laser excitation, and thus a more significant loss of ILS signal.

To illustrate the consequence of the AA during fully integrated runs, an accurately aligned run (**Figure 5 A-C**) is compared with a failed run (**Figure 5 D-F**). Strong ILS signal up to 300 bases was detected as expected when the separation channel was well-aligned (**Figure 5A**), which led to the detection of strong signals in the other colors (10-plex PCR product) during ME (**Figure 5B**). This corroborated with the strong signals when the PCR product was injected on a conventional CE instrument (**Figure 5C**, *ABI 3130 xl*). In contrast, an integrated run overly mis-aligned in the X direction resulted in poor ILS signals that failed the analytical threshold of 134 RFU beyond ILS120 (**Figure 5D and inset**). Poor PCR signals were collected on ME (**Figure 5E**), even though PCR efficiency was excellent (as seen on CE, **Figure 5F**).

The success rate of AA in the integrated study was 92.3%, as shown in **Figure 4C**, suggesting that the AA strategy is robust for µTAS applications. Executing 50 scans and moving to the found location during AA was ~4 min, which constitute <10% of the total analysis time. Compared to the 16-capillary *ABI 3130 xl*, this conventional instrument takes 6 min to complete spatial alignment, but requires the user to evaluate the alignment profile based on peak height, marking of the top of the peak, peak shape, and spacing[17]).

Conclusions

The work here described a simple yet robust solution for a challenge rarely discussed in the LOC or µTAS literature – automated alignment (AA) for laser-induced fluorescence (LIF) detection. This AA strategy negates the use of extraneous dye, and instead, utilizes the innate signatures of the separation channel to locate the detection window. The characteristic Z and X opto-signatures, attainable from multiple batches of injected molded separation domain and separation polymer types, enabled us to tailor an algorithm to pinpoint a 50 x 50
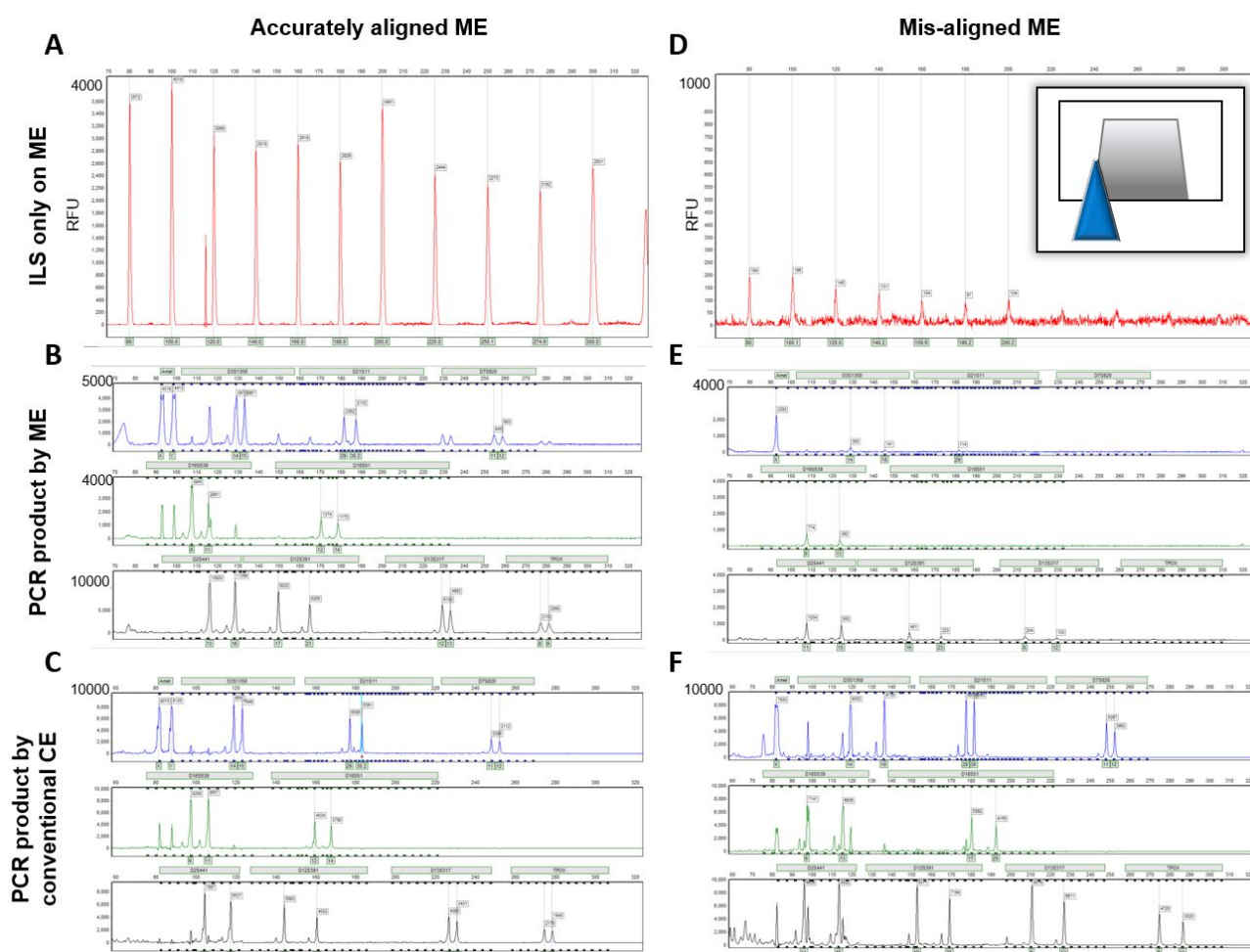
Figure 5 - Sample quality vs alignment position from fully automated and fully integrated analysis. (A) Strong ILS signal resulted from an accurately aligned ME. (B) Corresponding electropherogram of the run in the color channels for detecting PCR product. (C) The same PCR product injected on a conventional CE instrument (ABI 3130 xl). (D) Poor and incomplete ILS signal resulted from a mis-aligned ME. The inset shows the side view of the schematic of the optical alignment. (E) Corresponding electropherogram of the failed AA detected on ME. (F) The same PCR product injected on the CE showing successful PCR efficiency if channel was properly aligned. Electropherograms in B, C, E, and F show PCR products listed from left to right as follows. Top row (FAM channel, in blue): Amelogenin, D3S1358, D21S11, and D7S820. Middle row (JOE channel, in green): D16S539 and D18S51. Bottom row (F3TMR channel, in black): D2S441, D12S391, D13S317, and TPOX.

Page 9 of 11
Lab on a Chip
Please do not adjust margins

Journal Name

ARTICLE

µm channel within a vast 3D spatial arrangement. Once the algorithm was optimized, we conducted a systemic alignment study to establish the success metric for AA. Four alignment scenarios were investigated for their impact on signal strength, and determined that mis-alignment in the X direction (Scenario 2) is less disruptive than the Z direction (Scenario 3). Significant signal loss was observed when mis-alignment in both directions occurred (Scenario 4), though the incidence was very rare. The AA algorithm proved reproducible with a success rate of 92% from 26 fully integrated DNA analysis runs. The time to perform AA was 4 min, which took up <10% of the total analysis time. Future studies will involve understanding the failure modes and refining the AA strategy and algorithm to further improve the success rate.

The initial data reported here is an important piece of the puzzle to bringing our Rapid DNA instrument to completion. Previously, we have made progress in chip fabrication using the PCL method[12, 14], rapid DNA liberation on chip[18], multiplex PCR on chip[19, 20], and ME[13] for the purpose of DNA typing for human identification. The addition of AA is a monumental step towards realizing a truly automated and integrated µTAS for non-trained individuals, and a major component that advanced our technology to TRL7. The beauty of this AA implementation goes beyond simplicity in assay design, but also in its hardware requirement. The entire AA process operated from hardware already built for LIF, thus eliminating the requirement for additional sensors or alignment equipment, which provided significant reduction in manufacturing cost, and volumetric and weight footprint (the latter two were important considerations for an ultra-portable instrument). The dynamic nature of the algorithm seeks the separation channel for each run, allowing minuscule manufacturing and assembling errors in the microchip. Even as the microchip evolves beyond TRL7 to minimize manufacturing errors, potentially with entirely injected molded microchip, dynamic alignment is still expected, as we have seen in previous work.[6, 7] Furthermore, dynamic AA acts as a hardware calibration prior to each run for a system designed to be highly portable, analogous to calibrations done whenever bench-top genetic analyzers are transported. The added benefit of a fully closed instrument is important for laser safety for the operator, especially one such as this which was designed for non-expert users. This represents the first report describing a fluorescence-free alignment method for ME and, equally important, the first description of AA on a centrifugal platform. The scope of AA beyond DNA typing is obvious, we hope readers with other analytical applications requiring fluorescent detection on a micro-fabricated device find this useful.

Conflicts of interest

There are no conflicts to declare.

Acknowledgements

References

1.   P. A. Willis, J. S. Creamer and M. F. Mora, *Analytical and Bioanalytical Chemistry*, 2015, **407**, 6939-6963.
2.   J. Butler, *Fundamentals of Forensic DNA Typing*, Elsevier, San Diego, United States, 2009.
3.   P. Corporation, *Journal*, 2017.
4.   Federal Bureau of Investigation, Rapid DNA, https://www.fbi.gov/services/laboratory/biometric-analysis/codis/rapid-dna, (accessed July 15, 2019).
5.   W. A. Ausserer, L. Bousse, S. J. Gallagher, C. B. Kennedy and H. L. Phan, *JALA: Journal of the Association for Laboratory Automation*, 2001, **6**, 69-72.
6.   E. Tan, R. S. Turingan, C. Hogan, S. Vasantgadkar, L. Palombo, J. W. Schumm and R. F. Selden, *Investigative Genetics*, 2013, **4**, 16.
7.   D. Le Roux, B. E. Root, J. A. Hickey, O. N. Scott, A. Tsuei, J. Y. Li, D. J. Saul, L. Chassagne, J. P. Landers and P. de Mazancourt, *Lab on a Chip*, 2014, **14**, 4415-4425.
8.   A. J. Hopwood, C. Hurth, J. Yang, Z. Cai, N. Moran, J. G. Lee-Edghill, A. Nordquist, R. Lenigk, M. D. Estes, J. P. Haley, C. R. McAlister, X. Chen, C. Brooks, S. Smith, K. Elliott, P. Koumi, F. Zenhausern and G. Tully, *Analytical Chemistry*, 2010, **82**, 6991-6999.
9.   United States Patent. US 5,614,726, 1997.
10.   United States Patent. US 5,208,466, 1993.
11.   A. Scott, C. Birch, C. Clark, T. Layne, D. Le Roux, J. Li, D. Mills, D. Nelson, S. Panesar, M. Startseva, B. Thompson, B. Root and J. Landers, unpublished work.
12.   B. L. Thompson, Y. Ouyang, G. R. M. Duarte, E. Carrilho, S. T. Krauss and J. P. Landers, *Nature Protocols*, 2015, **10**, 875-886.
13.   B. L. Thompson, C. Birch, D. A. Nelson, J. Y. Li, J. A. DuVall, D. Le Roux, A. C. Tsuei, D. L. Mills, B. E. Root and J. P. Landers, *Lab on a Chip*, 2016, **16**, 4569-4580.
14.   C. Birch, J. A. DuVall, D. Le Roux, B. L. Thompson, A. C. Tsuei, J. Y. Li, D. A. Nelson, D. L. Mills, J. P. Landers and B. E. Root, *Micromachines*, 2017, **8**.
15.   F. B. o. Investigation, CODIS and NDIS fact sheet, https://www.fbi.gov/services/laboratory/biometric-analysis/codis/codis-and-ndis-fact-sheet, (accessed August 27, 2019).
16.   N. I. o. S. a. Technology, Overview of STR Fact Sheets, https://strbase.nist.gov/str_fact.htm, (accessed August 27, 2019).
17.   Applied Biosystems 3130/3130xl Genetic Analyzers Getting Started Guide, https://tools.thermofisher.com/content/sfs/manuals/4477796.pdf, (accessed June 4, 2019).
18.   B. L. Thompson, C. Birch, J. Y. Li, J. A. DuVall, D. Le Roux, D. A. Nelson, A. C. Tsuei, D. L. Mills, S. T. Krauss, B. E. Root and J. P. Landers, *Analyst*, 2016, **141**, 4667-4675.
19.   J. A. DuVall, D. Le Roux, A. C. Tsuei, B. L. Thompson, C. Birch, J. Li, D. A. Nelson, D. L. Mills, M. M. Ewing, R. S.

Please do not adjust margins
Lab on a Chip
Page 10 of 11

McLaren, D. R. Storts, B. E. Root and J. P. Landers, *Analytical Methods*, 2016, **8**, 7331-7340.

20.   J. A. DuVall, D. Le Roux, B. L. Thompson, C. Birch, D. A. Nelson, J. Y. Li, D. L. Mills, A. Tsuei, M. G. Ensenberger, C. Sprecher, D. R. Storts, B. E. Root and J. P. Landers, *Analytica Chimica Acta*, 2017, **980**, 41-49.

5

An automated alignment method was optimized for maximizing laser-induced fluorescence detection in a total DNA analysis system, using innate opto-signatures from microchannel features.